

ITS-90 Non-uniqueness from PRT Subrange Inconsistencies over the Range 24.56 K to 273.16 K

C.W. Meyer and W.L. Tew

*National Institute of Standards and Technology
Gaithersburg, Maryland, USA*

Abstract: We have performed calculations to study ITS-90 non-uniqueness from subrange inconsistencies over the range 24.5561 K to 273.16 K, where the scale is defined by an interpolating platinum resistance thermometer (PRT) that is calibrated via sets of defined fixed points. For this work, subrange inconsistency calculations have been performed on eighteen PRTs; fourteen are standard PRTs and four are miniature PRTs. The inconsistency uncertainties, which result from propagation of fixed-point uncertainties, have also been calculated. The calculations show that PRT subrange inconsistencies in the temperature region studied can be as large as 1 mK. We have also studied possible correlations between PRT subrange inconsistencies and other PRT properties/parameters that are simpler to determine; these studies show that there is a correlation between the average magnitude of the inconsistencies and the value of a certain calibration coefficient. Finally, for the range studied we have used a statistical analysis on the inconsistencies of the PRT ensemble to calculate a standard uncertainty to the ITS-90 temperature T_{90} due to the inconsistencies. Over the temperature intervals $25\text{ K} \leq T_{90} \leq 50\text{ K}$ and $100\text{ K} \leq T_{90} \leq 200\text{ K}$, this uncertainty dominates those propagated from fixed-point uncertainties.

1. Introduction

The ITS-90 is defined over the range 13.8033 K to 1234.93 K by means of a Platinum Resistance Thermometer (PRT) that is calibrated at specified sets of defining fixed points. [1] Temperature is determined from the resistance ratio

$$W(T_{90}) \equiv R(T_{90})/R_{\text{TPW}}, \quad 1)$$

where R is the PRT resistance at the ITS-90 temperature T_{90} and R_{TPW} is the resistance at the triple point of water (TPW). For calculating T_{90} from W , a calibration-dependent deviation function $D(T_{90})$ is used to relate W to an ITS-90 reference function $W_r(T_{90})$ [1]

$$W_r(T_{90}) = W(T_{90}) - D(T_{90}). \quad 2)$$

During calibration at fixed point i with scale-defined temperature $T_{\text{FP},i}$ W is measured to obtain the fixed-point resistance ratio

$$W_{\text{FP},i} \equiv R_{\text{FP},i} / R_{\text{TPW}} \quad 3)$$

where $R_{\text{FP},i} = R(T_{\text{FP},i})$. Afterwards, the values of the $W_{\text{FP},i}$ are used to determine the coefficients for D .

For a PRT to qualify as a defining interpolating instrument, the ITS-90 requires that the sensor coil be made from pure, strain-free platinum and that $W(234.3156 \text{ K}) \leq 0.844235$ or $W(302.9146 \text{ K}) \geq 1.11807$. [1] These criteria are intended to assure a high degree of uniformity and accuracy in the interpolation characteristics. From this point on, all discussion of PRTs in this paper refers to those that satisfy the numerical qualification for being defining interpolating instruments. PRTs that exhibit a high degree of stability and reproducibility (variations at the TPW less than 0.2 mK) are generally identified as “Standard Platinum Resistance Thermometers” (SPRTs). The vast majority of PRTs used to realize the ITS-90 are indeed SPRTs. However, other PRTs that satisfy the ITS-90 numerical qualification but are not stable enough to be SPRTs are still manufactured and used for scale realization.

Within the PRT-defined range the ITS-90 specifies eleven subranges. [1] For each subrange k (here, we use the NIST subrange numbering method [2]), there is defined a unique functional form for $D(T_{90})$ (denoted $D_k(T_{90})$) and a unique subset of ITS-90 fixed points. Usually a PRT is calibrated only over one subrange—the smallest subrange that covers all temperatures the PRT is expected to measure—in order to save the user from unnecessary expenses. All PRT sub-ranges have regions of overlap with at least one other subrange, and all subranges are considered to have equal status by the ITS-90. Because the different D_k are constructed using different functional forms and fixed points, there are usually small inconsistencies between the different D_k between fixed points due to different interpolations. These inconsistencies result in temperature-interpolation differences known as “subrange inconsistencies” or “Type 1 non-

uniqueness” in the ITS-90 [3-5]. The ITS-90 temperature determined using subrange k is $T_{90,k}$, and the subrange inconsistency $I_{j,k}$ between $T_{90,j}$ and $T_{90,k}$ is defined as

$$I_{j,k} \equiv T_{90,j} - T_{90,k} \quad . \quad 4)$$

Assuming $I_{j,k} \ll T_{90}$ and $D \ll W$, the subrange inconsistency may be approximated as

$$I_{j,k} \cong -\frac{\partial T_{90}}{\partial W}(D_j - D_k) \cong -\frac{\partial T_{90}}{\partial W_r}(D_j - D_k) \quad 5)$$

Subrange inconsistencies are one of three principal types of interpolation uncertainties of PRTs. A second type is from interpolation inconsistencies between different PRTs (all of which provide equally valid realizations of the ITS-90); this is known as “Type 3 non-uniqueness”. [5] The third and principle type of uncertainty arises from the normal propagation of fixed-point uncertainties during the interpolation. [6-8] All must be considered and characterized to properly estimate the uncertainties for temperature measurement on the ITS-90 using PRTs. Uncertainty contributions from non-uniqueness usually are not included in uncertainty estimates for PRTs in their calibration reports. However, these non-uniqueness contributions are often included in the PRT uncertainty budget when reporting studies comparing T_{90} to the thermodynamic temperature [9].

Calibrations of PRTs over the four ITS-90 sub-ranges below 273.16 K involve measurement of $W_{FP,i}$ for different combinations of eight fixed points. These eight fixed points are all triple points (TP) with the exception of two points near 17 K and 20.27 K. These eight assigned fixed-point temperatures are listed in Table 1 along with the gallium melting point (Ga MP). The four sub-ranges below 273.15 K and their corresponding fixed points are shown in Table 2.

While several studies have been performed on the magnitude of subrange inconsistencies for the range $273.16 \text{ K} \leq T_{90} \leq 1234.93 \text{ K}$ [10-15], only three previous studies have been published [3,4,16,17] for the region $13.8033 \text{ K} \leq T_{90} \leq 273.16 \text{ K}$. In the first of these studies, Hill and Bedford [3] calculated $I_{1,4}$ for six SPRTs according to variations in the assignment of the Hg TP temperature. The same calibration data were later updated and presented in the ITS-90 supplement [4] with calculations of $I_{1,2}$, $I_{1,3}$ and $I_{1,4}$. In the second study, $I_{1,4}$ was calculated for 11 PRTs calibrated at the National Physical Laboratory (UK) and presented in a publication by Working Group 3 of the Consultative Committee on Thermometry (CCT). [16] More recently, Steele [17] reported on calculations of sub-range inconsistencies between the same sub-range combinations using data derived from the CCT Key Comparison 2 (K2) [18]. In that work, 13 capsule SPRTs were studied as supplied by seven National Metrology Institutes (NMIs). Two of the SPRTs included in this study (serial numbers 1774095 and 1774092) were also included in Steele's calculations.

In this paper we report our determinations of subrange inconsistencies over this low-temperature region for fourteen capsule-type SPRTs and four miniature capsule PRTs. All of these

thermometers were calibrated at the National Institute of Standards and Technology (NIST). The subrange inconsistencies calculated are $I_{1,2}$, $I_{1,3}$, $I_{1,4}$, $I_{2,3}$, $I_{2,4}$ and $I_{3,4}$. We calculate the uncertainty $u(I_{j,k})$ of each subrange inconsistency; this uncertainty is propagated from those uncertainties of the fixed-point resistance ratios $u(W_{FP,i})$. We also compare the values of $I_{j,k}$ to those of the propagated uncertainties from the fixed-point calibrations; this compares the PRT temperature-measurement uncertainty resulting from subrange inconsistency to that from its actual calibration. In addition, we examine possible correlations between the inconsistencies and other properties of the PRTs under investigation. Finally, for the range studied we use a statistical analysis on the PRT ensemble to calculate a standard uncertainty to T_{90} due to PRT subrange inconsistencies.

2. Indicators for Chemical Purity of the Platinum in a PRT

The deviations $D(T_{90})$ for any particular PRT are one measure of the chemical purity of the platinum wire element, with smaller values of $D(T_{90})$ corresponding to higher purity. For $T_{90} < 273.16$ K, $D(T_{90})$ is most often positive. However, negative values of $D(T_{90})$ have also been observed in some PRTs over this range; the platinum in these thermometers has even higher purity than that in the PRTs used to construct the reference function $W_r(T_{90})$.

Another measure of chemical purity is the residual resistance ratio \mathcal{R} [19], which for platinum can be written as

$$\mathcal{R} = \frac{R(273.15 \text{ K})}{R(4.22 \text{ K})} \cong \frac{0.99996}{W(4.22 \text{ K})}. \quad 6)$$

Samples of platinum with higher \mathcal{R} values are of higher chemical purity and also have fewer lattice defects. In general, for capsule-type SPRTs that can measure \mathcal{R} , this value is a more sensitive measure of defects such as crystal strain than are either $W(\text{Hg TP})$ or $W(\text{Ga MP})$. The use of \mathcal{R} also allows comparison to data in the archival literature on other samples of platinum.

3. Platinum Thermometers

A total of 18 thermometers were used for this study. All thermometers satisfied the ITS-90 criteria $W(\text{Hg TP}) \leq 0.844235$ and $W(\text{Ga MP}) \geq 1.11807$ for a PRT to qualify as a defining interpolating instrument for the sub-ranges below 273.15 K. Of the 18 PRTs, 14 are capsule-type SPRTs with $R(273.16 \text{ K}) \approx 25.5 \Omega$ from 4 different commercial sources. In addition, we performed calculations for 4 miniature capsule PRTs with $R(273.16 \text{ K}) \approx 100 \Omega$, taken from a fifth commercial source and designated here as MPRTs. This particular combination of samples was chosen to represent both those SPRTs maintained by NIST and those SPRTs and MPRTs which are routinely calibrated at NIST for customers over the cryogenic range of temperatures. Efforts were made to include a diverse collection of thermometers such that the $W(\text{Hg TP})$ values

were distributed over more than 70 % of the range within the ITS-90 acceptance criteria. The entire set of sample platinum thermometers is summarized in Table 3.

The thermometers of type A construction included in this work are of the well known helical coil design derived from the work of Meyers [23] These were commercially produced until the mid-1980s, but are now no longer available. However, many of these SPRTs are still in wide use today, especially within the NMIs. Eight of the nine type A SPRTs included in this study are NIST check SPRTs used for ITS-90 maintenance and dissemination activities for $T_{90} \leq 83.8$ K. [24] The serial numbers for these SPRTs are 1774092, 1774095, 1004131, 1842382, 1842385, 1812279, 1812282, 1812284.

The two type B SPRTs used in this study are of a well established commercial design [25] and are taken from the Standard Reference Material (SRM) 1750 collection [21]. The Pt element is composed of parallel linear filaments of wire, mounted in bores of an alumina insulator and encapsulated in an all-metal sheath. The two samples chosen here, serial numbers 4463 and 4492, represent the lowest and second highest deviations $D(T_{90})$, respectively, from the ITS-90 reference function amongst the twenty SPRTs in the SRM 1750 population.

The single example of a type C SPRT included here, serial number 103, is a contemporary version of the classic helical coil design. This type is encapsulated in an all-glass sheath and is commercially available. The two type D SPRTs included here (serial numbers RS85A-9 and RS954-9) are also of a well established commercial helical coil design.

The MPRTs (type E) included in this study are derived from a well-established miniature coiled element design [22]. The data are taken from calibrations of both NIST and NIST-customer thermometers. These are calibrated in the same manner as are the capsule SPRTs; however, their self-heating characteristics are very different from, and they are inherently less reproducible than, most SPRTs. Hence, the uncertainties for the MPRT calibrations are somewhat larger than for the SPRT calibrations. The non-uniqueness characteristics of the four MPRTs included here are therefore presented separately.

4. Calibration Methods

The SPRTs and MPRTs involved in this work were all calibrated at NIST. For those fixed points within the range $13.8033 \text{ K} \leq T_{90} \leq 83.8058 \text{ K}$, the thermometers were calibrated within the NIST Low Temperature Calibration Facility (LTCF) and/or Low Temperature Realization Facility (LTRF) [24,26]. The Hg TP and TPW calibration data were obtained using immersion cells in the NIST SPRT Calibration Laboratory [27]. Four of the NIST check SPRTs were originally calibrated by direct realization of the fixed points below 83.8 K in the LTRF [28]. The remaining SPRTs and MPRTs were calibrated by comparison against one or more of these NIST check SPRTs within the LTCF. Additional triple-point realizations were performed on the NIST check SPRTs within the LTCF using NIST sealed cells [24,26,29]. The data used for this work were compiled from approximately eight years of calibration work in these NIST facilities. For

certain thermometers older calibration data were replaced by the most recent data; the changes were generally within the uncertainties (with coverage factor $\kappa = 2$) of the data. These calibration data were then used to derive $W_{FP,i}$ values at the fixed point temperatures for each thermometer.

The SPRT and MPRT expanded calibration uncertainties assigned to these fixed points are shown in Table 4. The expanded uncertainty U is related to the standard uncertainty u by $U = \kappa u$. For the values in Table 4, $\kappa = 2$. In the case of the SPRT uncertainties, some allowance was made for the fact that the data spanned an eight year time period and that some of the older calibration data were slightly more uncertain than that derived from more recent fixed-point realizations. In order to simplify the analysis presented here, we treated all the SPRT data as having a single set of fixed-point uncertainties taken as the largest values applicable for each fixed point. In the case of the MPRTs, some degree of hysteresis can result during thermal cycling which limits the reproducibility of the TPW resistance in these thermometers; this is also the dominant source of uncertainty for their $W(\text{Hg TP})$ values.

The values of $W_{FP,i}$ were used to calculate the coefficients in the ITS-90 deviation functions. The deviation equations provided interpolated values for $D(T)$ for the regions between fixed points for each subrange. Shown in Fig. 1 are the values of $D_1(T)$ on sub-range 1 for all PRTs studied in this work. A significant variation in the magnitude and shape of the deviation curves is evident. This variation is similar to that for a set of seven capsule SPRTs used by Hill and Steele. [30] A more detailed presentation of these PRTs' deviation characteristics is seen in Figure 2.

Here the correlation of $D(\text{Hg TP})$ and $D(\text{Ga MP})$ is plotted, for all of the PRTs in this study for which Ga MP data was available, within the bounds of the ITS-90 criteria.

5. Uncertainty Calculations

The uncertainty of the subrange inconsistency, $u(I_{j,k})$ may be determined by [31]:

$$u(I_{j,k})^2 = \sum_i \left(\frac{\partial I_{j,k}}{\partial x_i} \right) u(x_i)^2 + 2 \sum_{i=1}^{n-1} \sum_{l=i+1}^n r_{i,l} \frac{\partial I_{j,k}}{\partial x_i} \frac{\partial I_{j,k}}{\partial x_l} u(x_i) u(x_l) \quad 7)$$

Here, the x_i are the relevant quantities contributing to the uncertainty of $I_{j,k}$, $r_{i,l}$ is the correlation coefficient between quantities x_i and x_l . Also, $u(x_i)$ is the uncertainty of x_i and n is the total number of fixed points used for calibration in the combination of subranges j and k . With $I_{j,k}$, the relevant quantities are the $W_{\text{FP},i}$. For calculating the exact uncertainty, the correlations between the $W_{\text{FP},i}$ must be taken into account, since they may share a common TPW measurement or at least a common TPW cell [32]. However, this results in a complicated expression for the uncertainty. If the uncertainties for the correlated quantities are much smaller than those for the uncorrelated quantities, a considerable simplification may be made by making an approximation that assumes that all the $W_{\text{FP},i}$ are uncorrelated [32]. Then all $r_{i,l}$ in Eq. 7 are zero, and differentiating Eq. 5 yields

$$u(I_{j,k})^2 = \sum_{i=1}^n \left(\frac{\partial I_{j,k}}{\partial W_{FP,i}} \right) u(W_{FP,i})^2 \cong \left(\frac{\partial T_{90}}{\partial W_r} \right)^2 \sum_{i=1}^n \left[\frac{\partial (D_j - D_k)}{\partial W_{FP,i}} \right]^2 u(W_{FP,i})^2 \quad 8)$$

For the fixed-point realization uncertainties estimated by NIST, this approximation is accurate to within 7%. The expanded inconsistency uncertainties $U(I_{j,k})$ were then calculated using $U(I_{j,k}) = \kappa u(I_{j,k})$ with $\kappa = 2$.

Comparisons were made of each $I_{j,k}$ to the PRT calibration uncertainties $u_c(T_{90,j})$ and $u_c(T_{90,k})$ propagated from the fixed-points for subranges j and k . These comparisons were made to gain perspective on the relative significance of the subrange inconsistencies on total PRT temperature measurement uncertainties $u(T_{90})$. The uncertainties $u_c(T_{90,k})$ are a major component of $u(T_{90})$. Using the approximation described above, the uncertainty $u_c(T_{90,k})$ is given by

$$u_c(T_{90,k})^2 = \left(\frac{\partial T_{90}}{\partial W_r} \right)^2 \sum_{i=1}^n \left(\frac{\partial D_k}{\partial W_{FP,i}} \right)^2 u(W_{FP,i})^2 \quad 9)$$

The expanded calibration uncertainties $U_c(T_{90,k})$ were then calculated using $U_c(T_{90,k}) = \kappa u_c(T_{90,k})$, with $\kappa = 2$.

6. Results

Calculations for $I_{j,k}$, $U(I_{j,k})$, $U_c(T_{90,j})$ and $U_c(T_{90,k})$ were made as a function of temperature over all six ranges of overlap for subrange 1 to subrange 4, for all 18 PRTs. The quantities were calculated at all integer temperatures (in kelvin units) and fixed-point temperatures within the ranges of overlap. At each temperature, the corresponding W_r value was used as a nominal W value for use in calculating the quantities.

Shown in Fig. 3 to Fig. 8 are the six subrange inconsistencies, respectively. All figures have four plots. In the a) and b) plots, the subrange inconsistency is plotted as a function of temperature for the fourteen SPRTs and four MPRTs, respectively, with each PRT represented by a unique curve (see legend). In the c) and d) plots, the maximum, minimum and average values of the magnitude of $I_{j,k}$ are plotted for the SPRTs and MPRTs, respectively. In the figures, the values of $I_{j,k}$ are zero at the fixed points; this is to be expected because no PRT interpolation occurs at these temperatures. Curves representing $U(I_{j,k})$, $U_c(T_{90,j})$ and $U_c(T_{90,k})$ are also shown in the c) and d) plots. For simplicity in the representation of $U_c(T_{90,j})$ and $U_c(T_{90,k})$, we plot $U_c(T_{90})$, which we define as the larger of $U_c(T_{90,j})$ and $U_c(T_{90,k})$:

$$\begin{aligned} U_c(T_{90}) &= U_c(T_{90,j}) & \text{if} & \quad U_c(T_{90,j}) > U_c(T_{90,k}) \\ U_c(T_{90}) &= U_c(T_{90,k}) & \text{if} & \quad U_c(T_{90,j}) \leq U_c(T_{90,k}) \end{aligned} \quad 10)$$

Table 5 and Table 6 present a summary of the subrange inconsistency results for the SPRTs and MPRTs, respectively. For each subrange combination, the table shows the maximum and median values of $|I_{j,k}|$ over the set of PRTs (which we denote as $|I_{j,k}|_{\max}$ and $|I_{j,k}|_{\text{med}}$, respectively), at the temperature where the extremum in $|I_{j,k}|$ occurs. The tables also provide for each subrange combination the number of SPRTs and MPRTs where $|I_{j,k}| > U(I_{j,k})$ and listings of the PRTs with the largest inconsistency.

The largest inconsistency found was $|I_{1,2}|_{\max}$ at ~ 30 K, which had a value of $|I_{1,2}|_{\max} = 0.9$ mK for the SPRTs and 1.0 mK for the MPRTs. The largest $|I_{j,k}|_{\text{med}}$ was also at this temperature and between these two subranges; here these values were $|I_{1,2}|_{\text{med}} = 0.32$ mK for the SPRTs and $|I_{1,2}|_{\text{med}} = 0.81$ mK for the MPRTs. For the SPRTs, the smallest $|I_{j,k}|_{\text{med}}$ at the extremum temperature was $|I_{1,3}|_{\text{med}}$ with a value of $|I_{1,3}|_{\text{med}} = 0.09$ mK at this temperature; this was also the case for the MPRTs. With the SPRTs, two subrange inconsistencies had $|I_{j,k}|_{\text{med}}$ values that were outside their uncertainties; they were $I_{1,2}$ and $I_{2,3}$. Two inconsistencies had values of $|I_{j,k}|_{\text{med}}$ that were approximately equal to their uncertainties; they were $I_{1,3}$ and $I_{2,4}$. The inconsistencies $I_{1,4}$ and $I_{3,4}$ had values of $|I_{j,k}|_{\text{med}}$ that were all significantly lower than their uncertainties. For the MPRTs, the inconsistency uncertainty was much higher than for the SPRTs, so only $I_{1,2}$ was significantly higher than its uncertainty. It is interesting that despite the inconsistency uncertainties being larger for the MPRTs than for the SPRTs, the values of $|I_{j,k}|_{\text{med}}$ for the two types of PRTs were similar.

The results here are consistent with those shown in other studies [3,4,16,17]. In the most recent of these works, Steele [17] provided similar calculations of $I_{1,2}$, $I_{1,3}$, and $I_{1,4}$ (presented as $I_{2,1}$, $I_{3,1}$, and $I_{4,1}$, respectively, which results in a sign change) for the K2 SPRTs. His calculations include two PRTs (1774092 and 1774095) that are used in this work. For his collection of PRTs, Steele found results similar to ours for $I_{1,2}$, but with one such SPRT (213865) exhibiting an even larger inconsistency than that calculated for any PRT treated in this work. The $I_{1,3}$ curves as calculated by Steele are also similar to ours, but do not exceed approximately 0.25 mK in magnitude. The $I_{1,4}$ curves for the K2 SPRTs as calculated by Steele are qualitatively similar to ours but several of those curves exhibit extrema significantly larger than those found in our samples. A closer match to our distribution of $I_{1,4}$ curves results for the K2 thermometers when they are recalculated to agree with the KCRV comparison W values, but one SPRT in the ‘Group B’ collection is still anomalously large. Steele also provides a set of $I_{1,4}$ curves for a group of seven NRC SPRTs; here again several of the curves have extrema significantly greater than any of those for the SPRTs in this study. Steele’s calculations of $I_{1,4}$ for SPRTs 1774092 and 1774095 differ from ours, but as before these disagreements are due to the subsequent adjustments of the W_{FP} values for those SPRTs.

Steele’s subrange-inconsistency values for the NIST SPRTs 1774095 and 1774092 sometimes differ slightly from ours. These disagreements are due to small adjustments to several of the two thermometers’ W_{FP} values made since their original 1997 calibration; the original W_{FP} values were used with K2. Since all adjustments made since then have been within the bounds of the fixed-point uncertainties in Table 4, the shift in the inconsistency values illustrates the sensitivity

of the inconsistency values to the W_{FP} values, as well as the degree to which these calculations can be equivocal.

7. Correlation Studies on the Inconsistencies

To study the possible correlation between a PRT's subrange inconsistencies and its chemical purity, an "average inconsistency magnitude" $|I|_{ave}$ over all six subranges was first determined for each SPRT and MPRT. An average inconsistency uncertainty $u(I)_{ave}$ over all six subranges was also calculated for the SPRTs and MPRTs. The average inconsistency magnitude was defined by

$$|I|_{ave} = \frac{1}{6} \sum_{j,k} |I_{j,k}|_{ave, range} \quad (11)$$

Here, $|I_{j,k}|_{ave, range}$ is the value of $|I_{j,k}|$ for one PRT averaged over the range of overlap of subranges j and k and mathematically defined by

$$|I_{j,k}|_{ave, range} = \frac{\int_{T_a}^{T_b} |I_{j,k}(T_{90})| dT_{90}}{(T_b - T_a)} \quad (12)$$

In Eq. 12, T_a and T_b are the low temperature limit and high temperature limit of the overlap for the subrange combination. Similarly, the average inconsistency uncertainty was defined by

$$u(I)_{\text{ave}} = \frac{1}{6} \sum_{j,k} u(I_{j,k})_{\text{ave, range}} \quad (13)$$

where

$$u(I_{j,k})_{\text{ave, range}} = \frac{\int_{T_a}^{T_b} u(I_{j,k}(T_{90})) dT_{90}}{(T_b - T_a)} \quad (14)$$

The expanded average inconsistency uncertainty is then $U(I)_{\text{ave}} = \kappa u(I)_{\text{ave}}$, where $\kappa = 2$.

The SPRTs with the largest total inconsistency were A1718619 and 1812282, with $|I|_{\text{ave}}$ values 0.18 mK and 0.15 mK, respectively. The MPRT with the largest total inconsistency was 572 with $|I|_{\text{ave}} = 0.16$ mK. Figure 1 points out these SPRTs and MPRTs using arrows in the plot of $D(T_{90})$.

Plots showing the correlations between $|I|_{\text{ave}}$ and each of two chemical-purity-related quantities were produced, and for both combinations a correlation coefficient ρ was calculated. First, $|I|_{\text{ave}}$ was plotted versus $D(\text{Hg TP})$ for all the PRTs. No clear correlation was detectable between

$|I|_{\text{ave}}$ and $D(\text{Hg TP})$; this was confirmed by a small value for the correlation coefficient: $\rho = 0.41$. A similar plot was made to examine the correlations between $|I|_{\text{ave}}$ and the residual resistance \mathcal{R} . There was also no clear correlation seen for this combination, and calculations yielded $\rho = 0.20$. The small correlations observed here indicate that the subrange inconsistencies of a PRT are not related to the chemical purity of the its platinum.

A second set of correlation plots was made to examine the relation between $|I|_{\text{ave}}$ and the calibration coefficients a_4 and b_4 used in the deviation function for subrange 4. This deviation function is [1]

$$D_4 = a_4[W(T_{90}) - 1] + b_4[W(T_{90}) - 1]\ln W(T_{90}), \quad (15)$$

where a_4 and b_4 are determined by the values of $W(T_{90})$ obtained at the Ar TP, Hg TP, and TPW. The coefficient a_4 is proportional to the slope of $D(W)$ at the TPW and the coefficient b_4 is related to the curvature of $D(W)$ between the Ar TP and the TPW. No clear relation was found to exist between $|I|_{\text{ave}}$ and a_4 , and the calculated correlation coefficient was $\rho = 0.42$. This is no, since a_4 is nearly proportional to $-D(\text{Hg TP})$. However, a strong correlation was found between $|I|_{\text{ave}}$ and b_4 , resulting in $\rho = 0.82$. The correlation plot of this is shown in Fig. 9; this plot displays $|I|_{\text{ave}}$ versus b_4 for all the PRTs. The SPRTs and MPRTs are represented as solid circles and open circles, respectively, and the dashed and dot-dashed lines indicate $U(I)_{\text{ave}}$ for the SPRTs and MPRTs, respectively. A similarly high correlation was found between b_4 and other

statistical parameters for $|I_{j,k}|$. For example, the coefficient for the correlation between b_4 and the maximum value of $|I_{j,k}|$ over its temperature range, averaged over the six subranges, was $\rho = 0.84$. This high level of correlation shows that a calibration over the range 84 K to 273 K provides a useful indication of how large the subrange inconsistencies will be for a PRT between 24 K and 273 K. Specifically, if $b_4 < -2 \times 10^{-5}$, the PRT is likely to exhibit relatively large inconsistencies.

8. ITS-90 Uncertainty from Subrange Inconsistencies

There has been considerable interest in the thermometry community for establishing a standard uncertainty component to T_{90} due to PRT subrange inconsistencies. The results presented above may be used to attempt to estimate this uncertainty. However, it must first be recognized that the definition of the ITS-90 prevents it from having an uncertainty that complies with the ISO *Guide for the Expression of Uncertainty in Measurement* (GUM) [31]. An uncertainty as described by the GUM estimates the limits to deviations of a measured value from its unique actual value. However, temperature uncertainty from subrange inconsistencies does not involve measurement uncertainties but rather uncertainties due to ambiguities in the scale definition, and the GUM does not address such uncertainties. Therefore any uncertainty ascribed to the ITS-90 PRT definition cannot be GUM-compliant and must be characterized in a different way.

By introducing a unique value for T_{90} for an individual PRT based upon the existing PRT definitions, a subrange inconsistency uncertainty component that approaches GUM compliance may be estimated. For an individual PRT l , we first define $T_{90,k,l}$ as the value of T_{90} realized for subrange k and for PRT l . We may then define the ITS-90 temperature for PRT l to be the average of the $T_{90,k,l}$ values, denoted as $T_{90,l}$:

$$T_{90,l} = \frac{1}{n} \sum_{k=1}^n T_{90,k,l} \quad (16)$$

Here, n is the number of valid subranges at the temperature in question. For subrange k , we may then define the standard uncertainty to $T_{90,k}$ from subrange inconsistencies, $u_{\text{inc}}(T_{90,k})$, as a standard deviation of the $T_{90,k,l}$ values from $T_{90,l}$. For an uncertainty estimate by an ensemble of N PRTs, $u_{\text{inc}}(T_{90,k})$ is then given by

$$u_{\text{inc}}(T_{90,k})^2 = \frac{1}{N-1} \sum_l^N (T_{90,k,l} - T_{90,l})^2 \quad (17)$$

We stress that in performing these calculations, we are not advocating a change in the PRT definition of the ITS-90 or a change in realization methods. Rather, we simply wish to define a meaning of temperature “uncertainty” from subrange inconsistencies by providing a unique value of T_{90} from which a deviation may be estimated.

Figure 10 shows $u_{\text{inc}}(T_{90,k})$ as a function of temperature for $k=1$ to $k=4$. For simplicity, the PRTs used for Fig. 10 are the combined ensemble of SPRTs and MPRTs. Note that the uncertainties for the different subranges are not equivalent. In fact, from $83.8058 \text{ K} \leq T_{90} \leq 234.3156 \text{ K}$ $u_{\text{inc}}(T_{90,1})$ is approximately half the value of $u_{\text{inc}}(T_{90,4})$.

Fifth order polynomial fits have been made to the $u_{\text{inc}}(T_{90,k})$ values for subranges $k=1$ to $k=4$ for the temperature intervals

- A: $24.5561 \text{ K} \leq T_{90} \leq 54.3584 \text{ K}$,
- B: $54.3584 \text{ K} \leq T_{90} \leq 83.8058 \text{ K}$,
- C: $83.8058 \text{ K} \leq T_{90} \leq 234.3156 \text{ K}$
- D: $234.3156 \text{ K} \leq T_{90} \leq 273.16 \text{ K}$.

The fits were made with the functional form

$$u_{\text{inc}}(T_{90,k}) / \text{mK} = \sum_{i=1}^5 \alpha_{ki} (T_{90} - T_0)^i \quad 18)$$

where the resulting fitting parameters are given in Table 7. The residuals to the fit were all less than $3 \mu\text{K}$.

Figure 11 shows the increases made to the total SPRT calibration uncertainty for subrange k by including $u_{\text{inc}}(T_{90,k})$. The figure shows plots for subrange 1 to subrange 4. Here the calibration uncertainties $u_c(T_{90,k})$ are calculated using Eq. 9 with NIST fixed-point uncertainties for SPRTs

(see Table 4). The expanded uncertainty $U_c(T_{90,k}) = 2u_c(T_{90,k})$ values are shown as the dashed curves. The solid curves show the quadrature sum of the dashed curve values and $U_{\text{inc}}(T_{90,k}) = 2u_{\text{inc}}(T_{90,k})$. Significant increases in the total uncertainty are apparent in regions of all four subranges, particularly for $25 \text{ K} \leq T_{90} \leq 50 \text{ K}$ and $100 \text{ K} \leq T_{90} \leq 200 \text{ K}$.

9. Summary

Subrange inconsistencies in the SPRT definition of the ITS-90 add uncertainty to temperature measurements made on this scale, and therefore it is important to characterize these inconsistencies. For fourteen capsule-type SPRTs and four capsule MPRTs calibrated at NIST, we have determined the values and uncertainties of the inconsistencies between the four ITS-90 SPRT subranges below the triple point of water. The inconsistencies are always zero at the fixed point temperatures, where the subranges are constrained to agree with each other, and so the maxima of the inconsistencies were generally located at temperatures halfway between fixed points. The inconsistencies were large in some PRTs but insignificant in others. The maximum value of the calculated PRT subrange inconsistencies was $0.98 \text{ mK} \pm 0.38 \text{ mK}$. There were no clear correlations between the average inconsistency magnitude for a PRT and its chemical-purity-related PRT parameters such as $W(\text{Hg TP})$ and the residual resistance. However, large correlations were observed between the average inconsistency magnitude for a PRT and its subrange 4 calibration parameter b_4 . Over small temperature ranges in the region 24 K to 273 K, the inconsistencies resulted in uncertainty contributions to T_{90} that dominated the PRT

calibration uncertainties. We calculated a standard uncertainty for T_{90} from subrange inconsistencies using statistical analysis on the data from this study. The appreciable size of these subrange inconsistencies over the temperature intervals $25 \text{ K} \leq T_{90} \leq 50 \text{ K}$ and $100 \text{ K} \leq T_{90} \leq 200 \text{ K}$ demonstrates the importance of including them as an uncertainty component for T_{90} .

Acknowledgements

We gratefully acknowledge D.R. White for encouraging us to do this work. We thank M.R. Moldover, G.F. Strouse, D.C. Ripple, D.R. White, and H.Y. Yoon for helpful discussions.

References

- [1] Preston-Thomas H 1990 *Metrologia* **27** 3-10,107
- [2] Mangum B W and Furukawa G T 1990 *NIST Technical Note 1265*
- [3] Hill K D and Bedford R 1989 *Document CCT/89-6* Bureau International des Poids et Mesures Consultative Committee for Thermometry
- [4] BIPM 1990 *Supplementary Information for the International Temperature Scale of 1990*, (Sèvres: Bureau International des Poids et Mesures)
- [5] Mangum B W, Bloembergen P, Chattle M V, Fellmuth B, Marcarino P and Pokhodun A I 1997 *Metrologia* **34** 427-429
- [6] Bloembergen P 1995/96 *Metrologia* **32** 253-257
- [7] Bloembergen P 1996 *Metrologia* **33** 269
- [8] White D R and Saunders P 2000 *Metrologia* **37** 285-293
- [9] Pitre L Moldover M R and Tew W L 2006 *Metrologia* **43** 142-162
- [10] Mangum B W, Pfeiffer E R and Strouse G F 1990 *Proceedings of TEMPMEKO* (Helsinki:TEMPMEKO) 17-36

- [11] Strouse G F 1992 *Temperature: Its Measurement and Control in Science and Industry* vol 5, ed J F Schooley (New York: AIP) 165-168
- [12] Moiseeva N P and Pokhodun A I 1992 *Temperature: Its Measurement and Control in Science and Industry* vol 5, ed J F Schooley (New York: AIP) 187-191
- [13] Ahmed M G 2004 *Proceedings of TEMPMEKO* (Cavtat:TEMPMEKO) 271-274
- [14] Zhiru K, Jingbo L and Xiaoting L *Metrologia* **21** 207-223
- [15] White D R and Strouse G F 2005 submitted to *Metrologia*
- [16] Crovini L et al. 1991 *Metrologia* **28** 317-325
- [17] Steele A G 2005 *Metrologia* **42** 289-297
- [18] Steele A G et al 2002 *Metrologia* **39** 551-571
- [19] Fickett F R 1983 *Materials at Low Temperatures*, ed R P Reed and A F Clark (Metals Park, Ohio: ASM) 163-196
- [20] Ward S D and Compton J P 1979 *Metrologia* **15** 31-46
- [21] Tew W L and Strouse G F 2001 NIST SP-260-139, US Govt. Printing Office
- [22] Lucas D A 1972 *Temperature: Its Measurement and Control in Science and Industry* vol 4, ed H H Plumb (Pittsburgh: ISA) 963-969
- [23] Meyers C H 1932 *J. Res. Nat. Bur. Stand.* **9** 807-813

- [24] Tew W L and Meyer C W, 2002 *Temperature: Its Measurement and Control in Science and Industry* vol 7, ed D C Ripple *et al* (Melville, New York: AIP Conf. Proc.) 143-148
- [25] Curtis D J 1972 *Temperature: Its Measurement and Control in Science and Industry* vol 4, ed H H Plumb (Pittsburgh: ISA) 951-961
- [26] Meyer C W and Tew W L 2002 *Temperature: Its Measurement and Control in Science and Industry* vol 7, ed D C Ripple *et al* (Melville, New York: AIP Conf. Proc.) 137-142
- [27] Strouse G F 1992 *Temperature: Its Measurement and Control in Science and Industry* vol 6, ed J F Schooley (New York: AIP) 169-174
- [28] Meyer C W and Reilly M L, *Proceedings of Low Temperature Thermometry and Dynamic Temperature Measurement*, ed A Szmyrka-Grzebyk (Wroclaw: IMEKO) L110-L115
- [29] Tew W L, Strouse G F, Meyer C W, and Furukawa G T 1998 *Advances in Cryogenic Engineering* **43B** ed P Kittel (New York: Plenum Press) 733-740
- [30] Hill K D and Steele A G 2005 *Metrologia* **42** 278-288
- [31] ISO 1993 *Guide to the Expression of Uncertainty in Measurement*, (Geneva, Switzerland: International Organization for Standardization)
- [32] Meyer C W and Ripple D C 2006, submitted to *Metrologia*

Table Captions

1. ITS-90 assigned fixed points for $13.8033 \leq T \leq 302.9146$ K and the corresponding notation used in this work.
2. Subranges for the PRT definition of the ITS-90 below 273.15 K.
3. Summary of platinum thermometers included in the present study. Types A through D are capsule SPRTs. Type E is a miniature capsule design. All thermometers satisfy ITS-90 criteria for being a defining interpolating instrument ($W(\text{Hg TP}) \leq 0.844235$ and $W(\text{Ga MP}) \geq 1.11807$).
4. Comparison and fixed-point expanded calibration uncertainties $U(W_{FP})$, for SPRTs and MPRTs where the coverage factor is $\kappa = 2$.
5. Summary of subrange inconsistency results for the 14 SPRTs. Uncertainties are a result of propagation of fixed-point uncertainties. The uncertainty values listed are expanded uncertainties with $\kappa = 2$.
6. Summary of subrange inconsistency results for the 4 MPRTs. As before, the uncertainty values listed are expanded uncertainties with $\kappa = 2$.
7. Fitting parameters for determining the uncertainty to T_{90} due to subrange inconsistencies for subrange 1 to subrange 4 from 24.5561 K to 273.16 K using Eq. 18. The standard

uncertainty is defined by Eq. 17. The labels A, B, C and D for the temperature intervals are described in the text above Eq. 18.

Figure Captions

1. Deviations $D_1 \equiv W - W_r$ as a function of temperature T_{90} for the entire set of eighteen PRTs, using the deviation function for subrange 1 [1]. Here, W is the resistance ratio of a SPRT at T and W_r is the ITS-90 reference function at that temperature. The black arrows indicate the three SPRTs with the largest overall subrange inconsistencies.
2. Correlation plot of $D(\text{Hg TP})$ and $D(\text{Ga MP})$ for 16 of the PRTs in this work. The dashed correlation line is from the SRM 1750 collection [21].
3. Subrange inconsistency $I_{1,2}$ between subranges 1 and 2 for the eighteen PRTs studied. Here, $I_{1,2} = T_{90,1} - T_{90,2}$, where $T_{90,j}$ refers to the value of T_{90} for subrange j . The inconsistency $I_{1,2}$ is shown as a function of T_{90} for a) the fourteen SPRTs and b) the four MPRTs. The maximum, minimum, and median values of the magnitude of $I_{1,2}$ are shown for c) the fourteen SPRTs and d) the four MPRTs. The expanded uncertainty $U(I_{1,2})$ and the expanded T_{90} uncertainty component from propagation of fixed-point errors, $U_c(T_{90})$, are also shown in c) and d) for the SPRTs and MPRTs, respectively, where the coverage factor is $\kappa = 2$. The curve for $U_c(T_{90})$, is represented by the larger of $U_c(T_{90,1})$ and $U_c(T_{90,3})$ at T_{90} .
4. Subrange inconsistency $I_{1,3}$ between subranges 1 and 3 for the eighteen PRTs studied. See Fig. 3 for a description of the plots.

5. Subrange inconsistency $I_{1,4}$ between subranges 1 and 4 for the eighteen PRTs studied.
See Fig. 3 for a description of the plots.
6. Subrange inconsistency $I_{2,3}$ between subranges 2 and 3 for the eighteen PRTs studied.
See Fig. 3 for a description of the plots.
7. Subrange inconsistency $I_{2,4}$ between subranges 2 and 4 for the eighteen PRTs studied.
See Fig. 3 for a description of the plots.
8. Subrange inconsistency $I_{3,4}$ between subranges 3 and 4 for the eighteen PRTs studied.
See Fig. 3 for a description of the plots.
9. Correlation plot between $|I|_{\text{ave}}$ and the subrange 4 calibration coefficient b_4 . Here, $|I|_{\text{ave}}$ is the subrange inconsistency magnitude averaged over all six subranges, for one PRT, as defined in Eq. 11. The SPRTs are represented by the solid circles and the MPRTs are represented by the open circles. The dashed and dot-dashed curves represent $U(I)_{\text{ave}}$ for the SPRTs and MPRTs, respectively, with coverage factor $\kappa = 2$. The correlation coefficient for the $|I|_{\text{ave}}$ and b_4 is $\rho = 0.82$.
10. Plot of the standard uncertainty $u_{\text{inc}}(T_{90,k})$ (as defined by Eq. 17) as a function of T_{90} . This estimate is determined by the data for the combined ensemble of SPRTs and MPRTs. The values of $u_{\text{inc}}(T_{90,k})$ are shown for the individual subranges $k=1$ to $k=4$. Note that for $24.5561 \text{ K} \leq T_{90} \leq 54.3584 \text{ K}$ the curves for subrange 1 and subrange 2 overlap.

11. Increases in the SPRT calibration uncertainty $u_c(T_{90,k})$ for subrange k resulting from including uncertainties due to subrange inconsistencies $u_{inc}(T_{90,k})$. Plots for subrange 1 to subrange 4 are shown. Here, $u_c(T_{90,k})$ is calculated using Eq. 9 using NIST fixed-point uncertainties for SPRTs (see Table 4). The dashed curves are the expanded uncertainty $U_c(T_{90,k}) = 2u_c(T_{90,k})$. The solid curves are the quadrature sum of the dashed-curve values and $U_{inc}(T_{90,k}) = 2u_{inc}(T_{90,k})$.

Table 1

Notation	Fixed Point	T_{90} / K
e-H ₂ TP	triple point of equilibrium hydrogen	13.8033
e-H ₂ VP1	equilibrium hydrogen vapor pressure point at 32.3213 kPa	17.035
e-H ₂ VP2	equilibrium hydrogen vapor pressure point at 101.292 kPa	20.27
Ne TP	triple point of neon	24.5561
O ₂ TP	triple point of oxygen	54.3584
Ar TP	triple point of argon	83.8058
Hg TP	triple point of mercury	234.3156
TPW	triple point of water	273.16
Ga MP	gallium melting point	302.9146

Table 2

Subrange Number	Temperatures Covered	Fixed Points Used
1	$13.08033 \text{ K} \leq T_{90} \leq 273.16 \text{ K}$	e-H ₂ TP, e-H ₂ VP1, e-H ₂ VP2, Ne TP, O ₂ TP, Ar TP, Hg TP, TPW
2	$24.5561 \text{ K} \leq T_{90} \leq 273.16 \text{ K}$	e-H ₂ TP, Ne TP, O ₂ TP, Ar TP, Hg TP, TPW
3	$54.3584 \text{ K} \leq T_{90} \leq 273.16 \text{ K}$	O ₂ TP, Ar TP, Hg TP, TPW
4	$83.8058 \text{ K} \leq T_{90} \leq 273.16 \text{ K}$	Ar TP, Hg TP, TPW

Table 3

Serial No.	Type	$D(\text{Hg TP}) / 10^{-5}$	\mathcal{R}	Comments
1004131	A	3.21	2115	
1718619	A	6.58	–	
1774092	A	0.50	3030	CCT K2, 1997-1999 [18]
1774095	A	3.86	2055	
1812279	A	2.38	2825	IPTS-68 Comparison [20]
1812282	A	3.21	2786	
1812284	A	3.16	2855	
1842382	A	–0.19	3149	Acoustic Determination [9]
1842385	A	0.69	2834	
4463	B	1.71	2324	SRM 1750 [21]
4492	B	2.38	2158	
103	C	2.13	2233	
RS85A-9	D	2.79	2370	
RS954-9	D	2.90	1899	
533	E	6.15	–	Miniature Capsules, 100 Ω [22]
534	E	6.54	1590	
571	E	4.42	1855	
572	E	6.30	1734	

Table 4

Fixed Point	SPRT $U(W_{FP})/\text{mK}$	MPRT $U(W_{FP})/\text{mK}$
e-H ₂ TP	0.37	0.37
e-H ₂ VP1	0.25	0.25
e-H ₂ VP2	0.20	0.20
Ne TP	0.31	0.31
O ₂ TP	0.15	0.16
Ar TP	0.22	0.27
Hg TP	0.25	0.49
TPW	0.14	0.52

Table 5

$I_{j,k}$	$ I_{j,k} _{\max}$ (mK) at extremum T_{90}	$ I_{j,k} _{\text{med}}$ (mK) at extremum T_{90}	$ I_{j,k} _{\text{med}}$ (mK) ave. over range	SPRTs with $ I_{j,k} > U(I_{j,k})$	SPRTs with largest inconsistency
$I_{1,2}$	0.89 ± 0.33	0.32 ± 0.33	0.04	9/14	1004131, 1812282
$I_{1,3}$	0.54 ± 0.09	0.09 ± 0.09	0.04	7/14	1718619, 1812284
$I_{1,4}$	0.63 ± 0.29	0.24 ± 0.29	0.10	2/14	1718619, 1812282
$I_{2,3}$	0.78 ± 0.08	0.11 ± 0.08	0.05	9/14	1718619, 1812284
$I_{2,4}$	0.85 ± 0.29	0.28 ± 0.29	0.13	5/14	1812279, 1812282
$I_{3,4}$	0.30 ± 0.22	0.14 ± 0.22	0.06	2/14	4492, 4463

Table 6

$I_{j,k}$	$ I_{j,k} _{\max}$ (mK) at extremum T_{90}	$ I_{j,k} _{\text{med}}$ (mK) at extremum T_{90}	$ I_{j,k} _{\text{med}}$ (mK) ave. over range	MPRTs with $ I_{j,k} > U(I_{j,k})$	MPRT with largest Inconsistency
$I_{1,2}$	0.98 ± 0.38	0.81 ± 0.38	0.05	3/4	572
$I_{1,3}$	0.18 ± 0.12	0.09 ± 0.12	0.04	2/4	534
$I_{1,4}$	0.63 ± 0.50	0.23 ± 0.50	0.11	1/4	572
$I_{2,3}$	0.15 ± 0.12	0.10 ± 0.12	0.05	2/4	533
$I_{2,4}$	0.55 ± 0.51	0.22 ± 0.51	0.11	1/4	572
$I_{3,4}$	0.58 ± 0.40	0.08 ± 0.40	0.04	1/4	572

Table 7

Interval	A	B	C	D
T_0	24.5561 K	54.3584 K	83.8058 K	234.3156 K
α_{11}	$1.226\ 72 \times 10^{-1}$	$1.035\ 03 \times 10^{-2}$	$5.937\ 67 \times 10^{-3}$	$4.292\ 53 \times 10^{-4}$
α_{12}	$-1.882\ 93 \times 10^{-2}$	$-9.836\ 57 \times 10^{-4}$	$-1.190\ 04 \times 10^{-4}$	$-8.511\ 44 \times 10^{-6}$
α_{13}	$1.162\ 74 \times 10^{-3}$	$4.041\ 73 \times 10^{-5}$	$9.798\ 45 \times 10^{-7}$	$-6.165\ 75 \times 10^{-8}$
α_{14}	$-3.320\ 79 \times 10^{-5}$	$-8.844\ 29 \times 10^{-7}$	$-4.117\ 01 \times 10^{-9}$	0
α_{15}	$3.612\ 10 \times 10^{-7}$	$8.185\ 25 \times 10^{-9}$	$7.437\ 45 \times 10^{-12}$	0
α_{21}	$1.226\ 72 \times 10^{-1}$	$1.469\ 65 \times 10^{-2}$	$8.179\ 35 \times 10^{-3}$	$1.121\ 23 \times 10^{-3}$
α_{22}	$-1.882\ 93 \times 10^{-2}$	$-1.225\ 28 \times 10^{-3}$	$-1.174\ 48 \times 10^{-4}$	$-2.418\ 84 \times 10^{-5}$
α_{23}	$1.162\ 74 \times 10^{-3}$	$4.421\ 59 \times 10^{-5}$	$5.216\ 56 \times 10^{-7}$	$-1.187\ 54 \times 10^{-7}$
α_{24}	$-3.320\ 79 \times 10^{-5}$	$-9.021\ 57 \times 10^{-7}$	$-6.277\ 18 \times 10^{-10}$	0
α_{25}	$3.612\ 10 \times 10^{-7}$	$8.088\ 77 \times 10^{-9}$	$-3.524\ 29 \times 10^{-13}$	0
α_{31}		$2.446\ 61 \times 10^{-2}$	$4.516\ 32 \times 10^{-3}$	$7.571\ 90 \times 10^{-4}$
α_{32}		$-2.176\ 72 \times 10^{-3}$	$-4.246\ 06 \times 10^{-5}$	$-1.631\ 14 \times 10^{-5}$
α_{33}		$8.410\ 30 \times 10^{-5}$	$-1.541\ 05 \times 10^{-7}$	$-8.058\ 81 \times 10^{-8}$
α_{34}		$-1.782\ 94 \times 10^{-6}$	$2.652\ 34 \times 10^{-9}$	0
α_{35}		$1.627\ 20 \times 10^{-8}$	$-7.178\ 17 \times 10^{-12}$	0
α_{41}			$1.262\ 90 \times 10^{-2}$	$9.616\ 22 \times 10^{-4}$
α_{42}			$-2.625\ 39 \times 10^{-4}$	$-1.952\ 92 \times 10^{-5}$
α_{43}			$2.322\ 29 \times 10^{-6}$	$-1.276\ 28 \times 10^{-7}$
α_{44}			$-1.071\ 72 \times 10^{-8}$	0
α_{45}			$2.110\ 43 \times 10^{-11}$	0

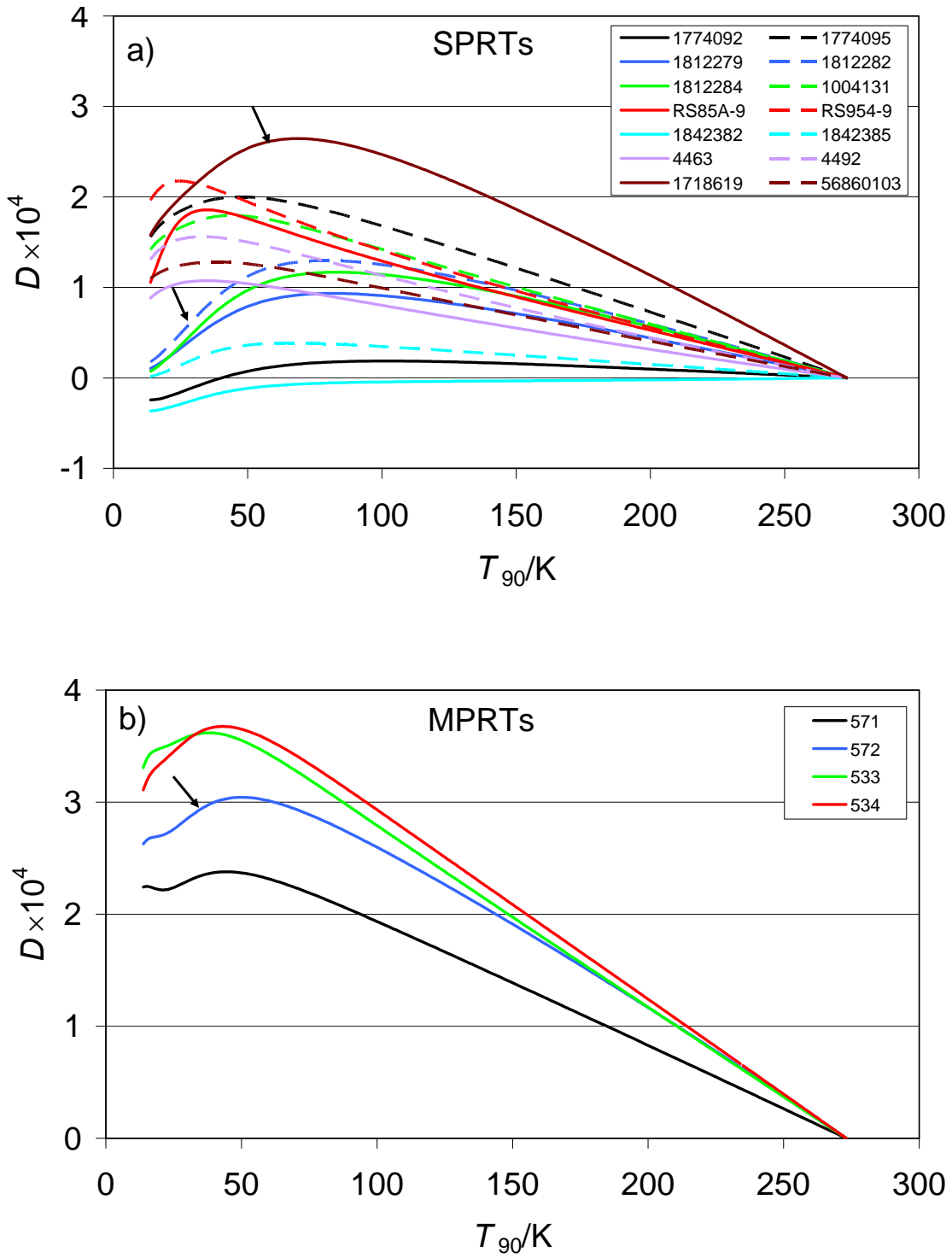


Figure 1

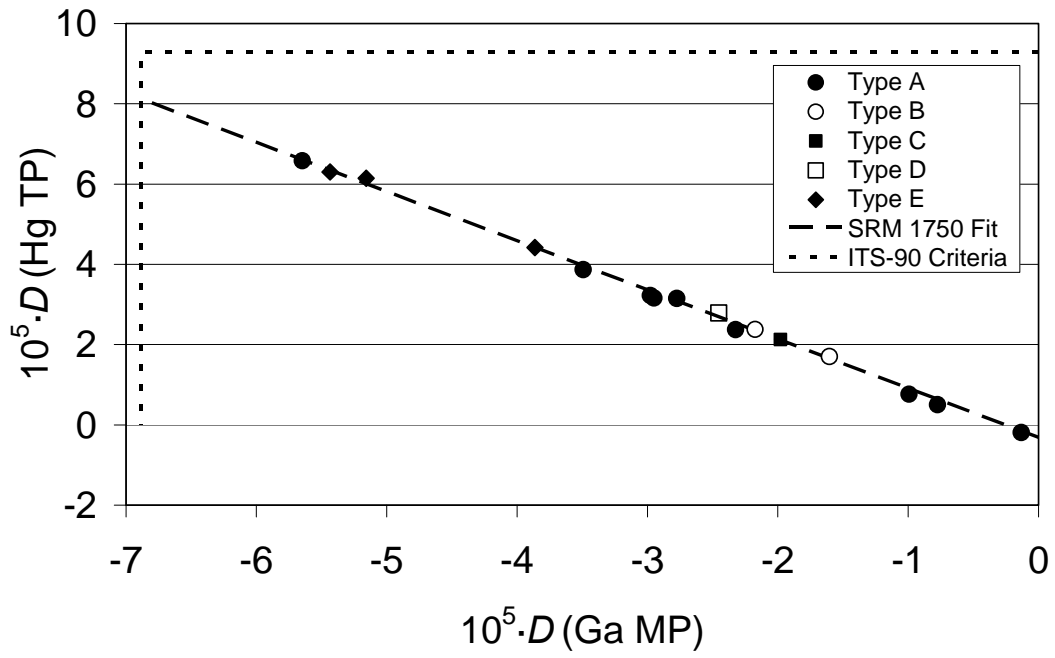


Figure 2

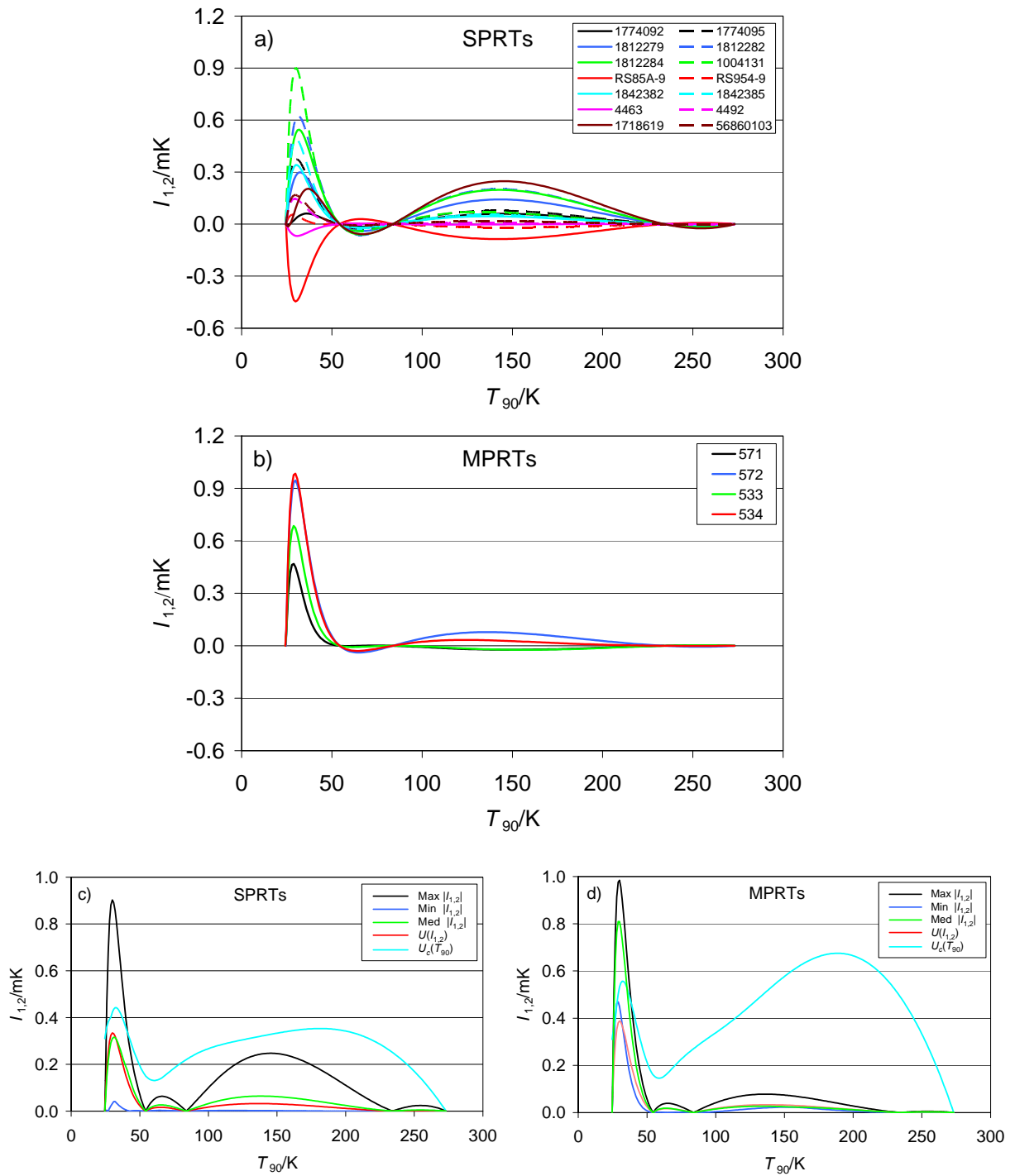


Figure 3

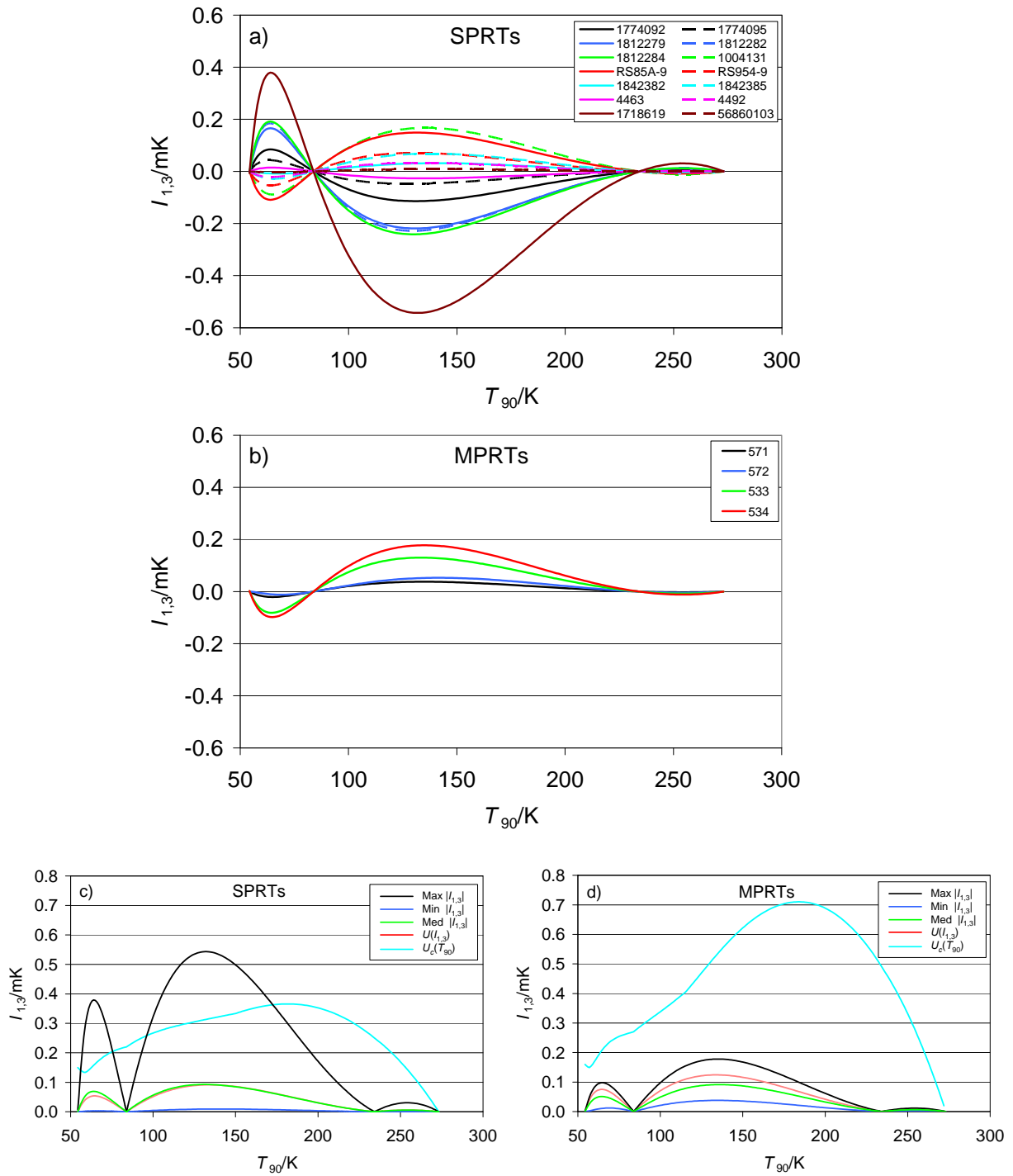


Figure 4

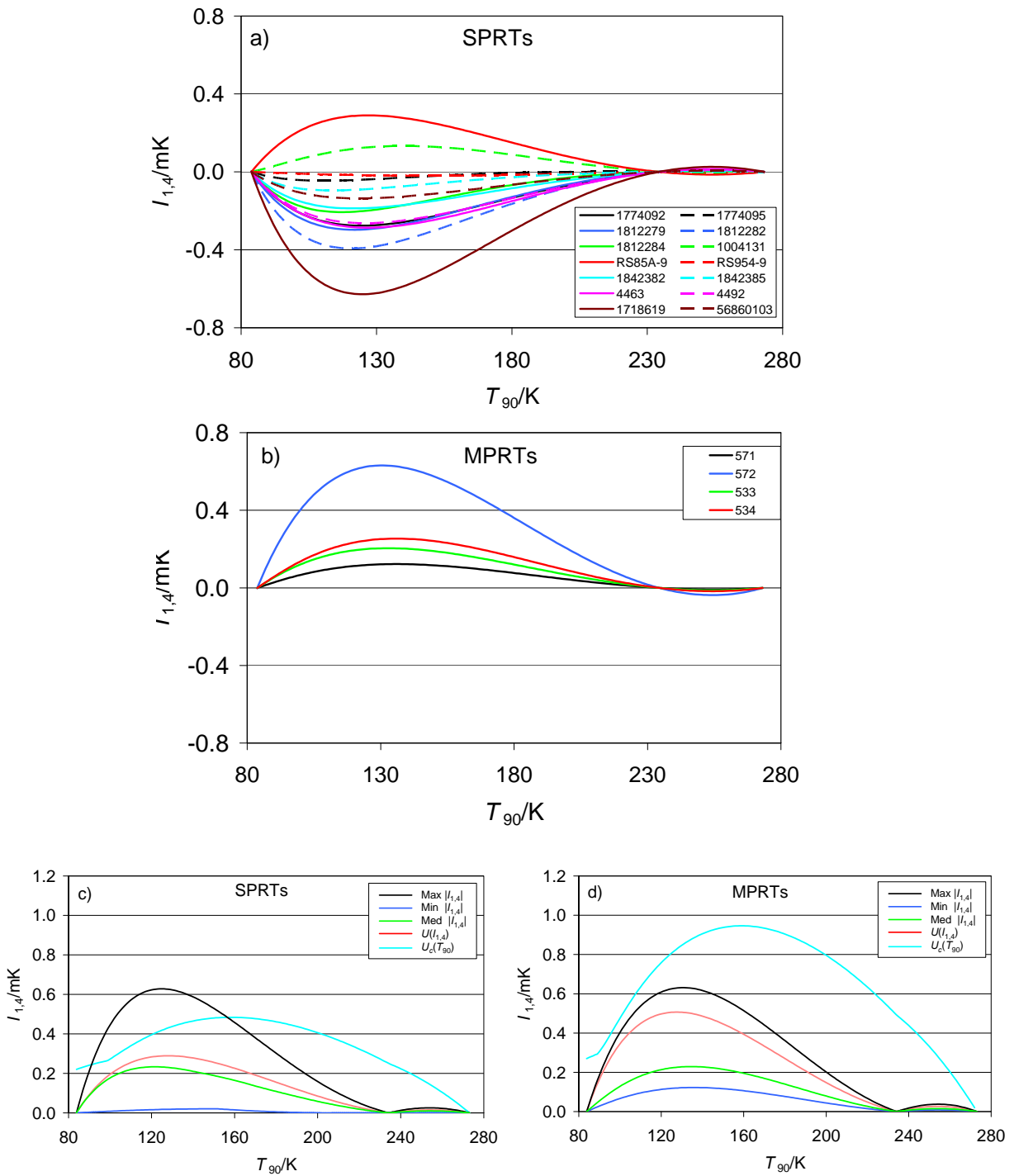


Figure 5

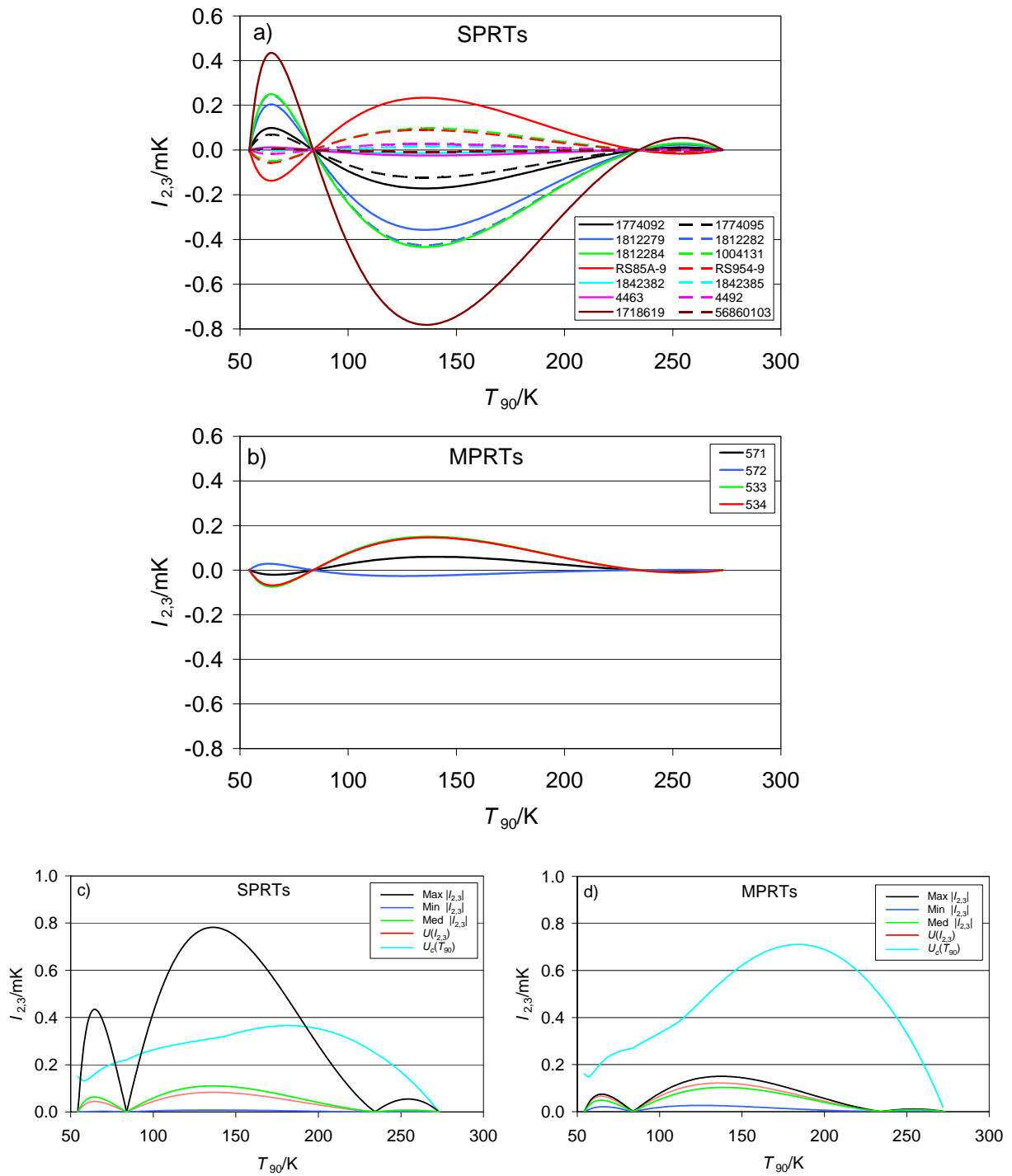


Figure 6

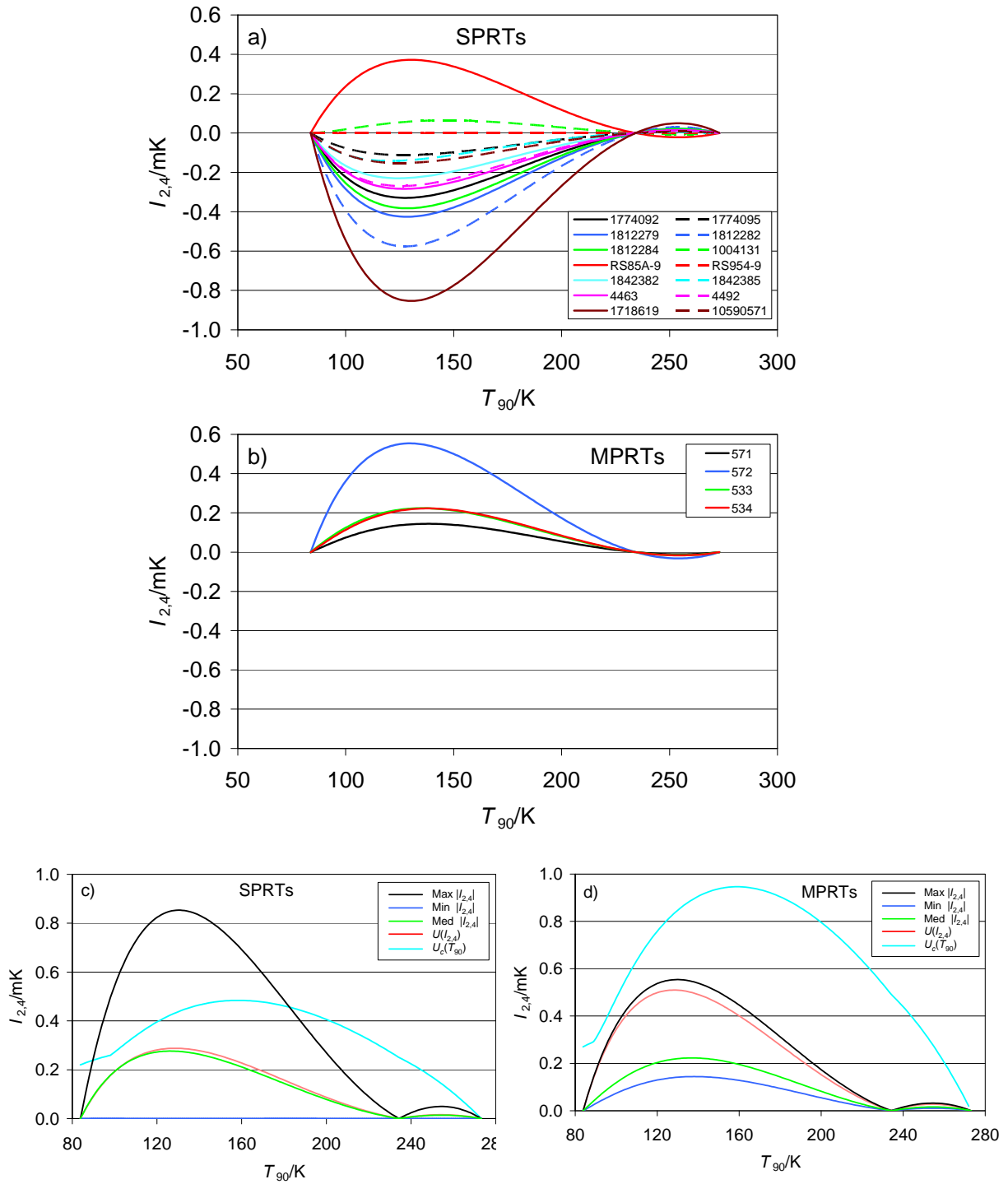


Figure 7

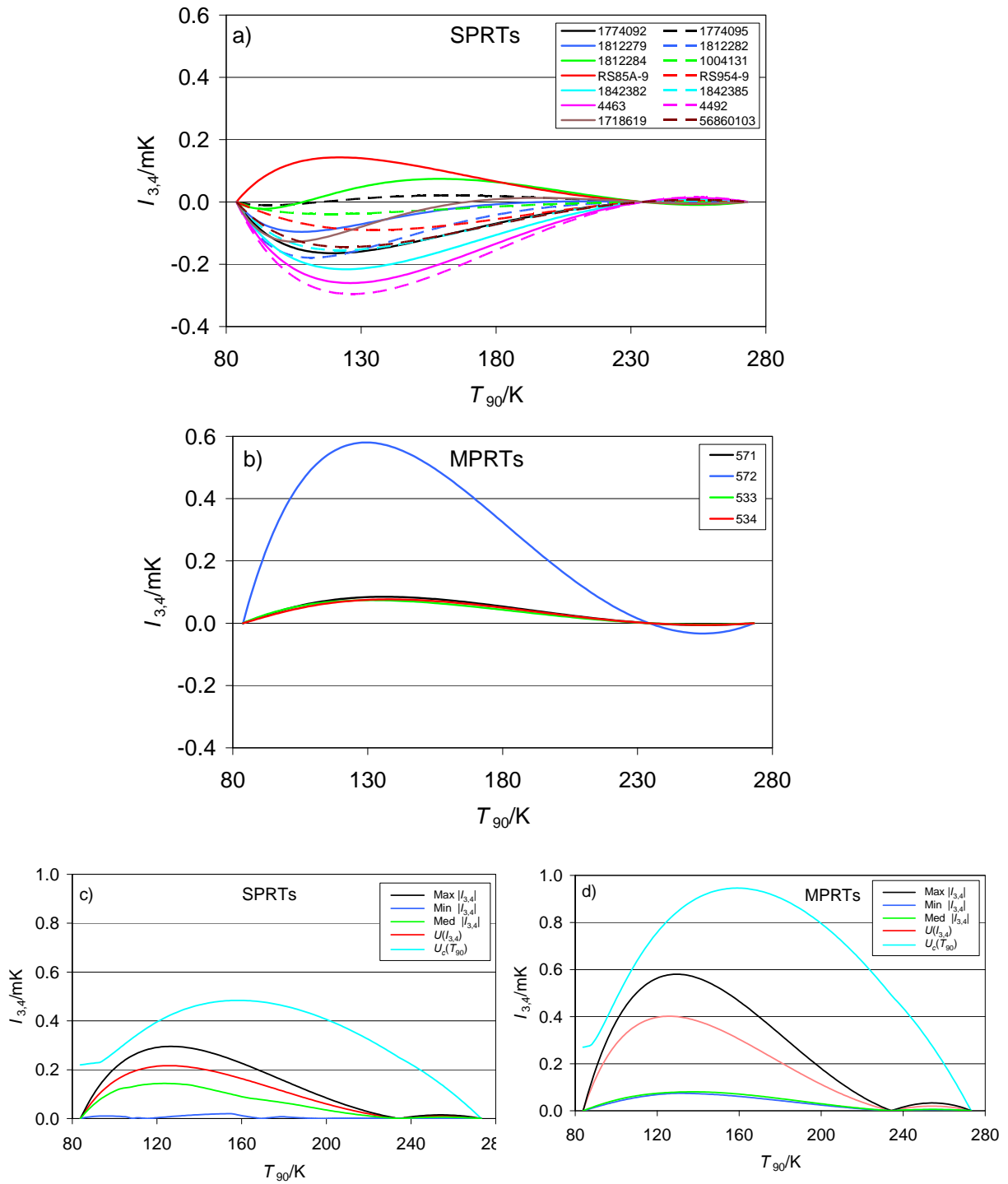


Figure 8

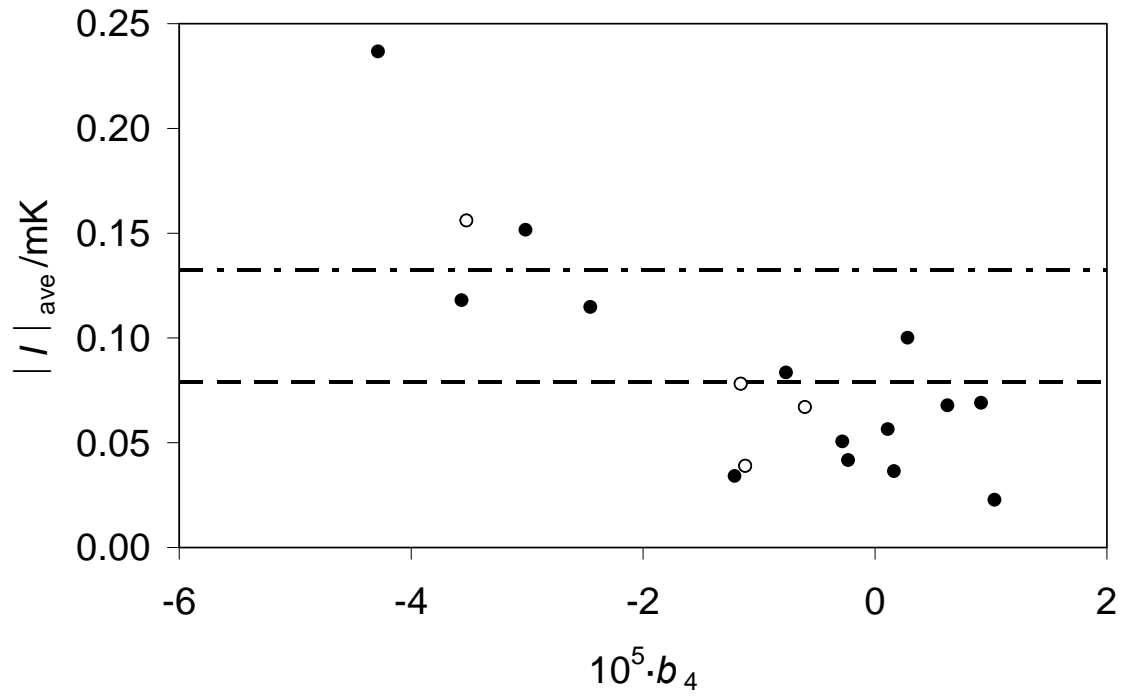


Figure 9

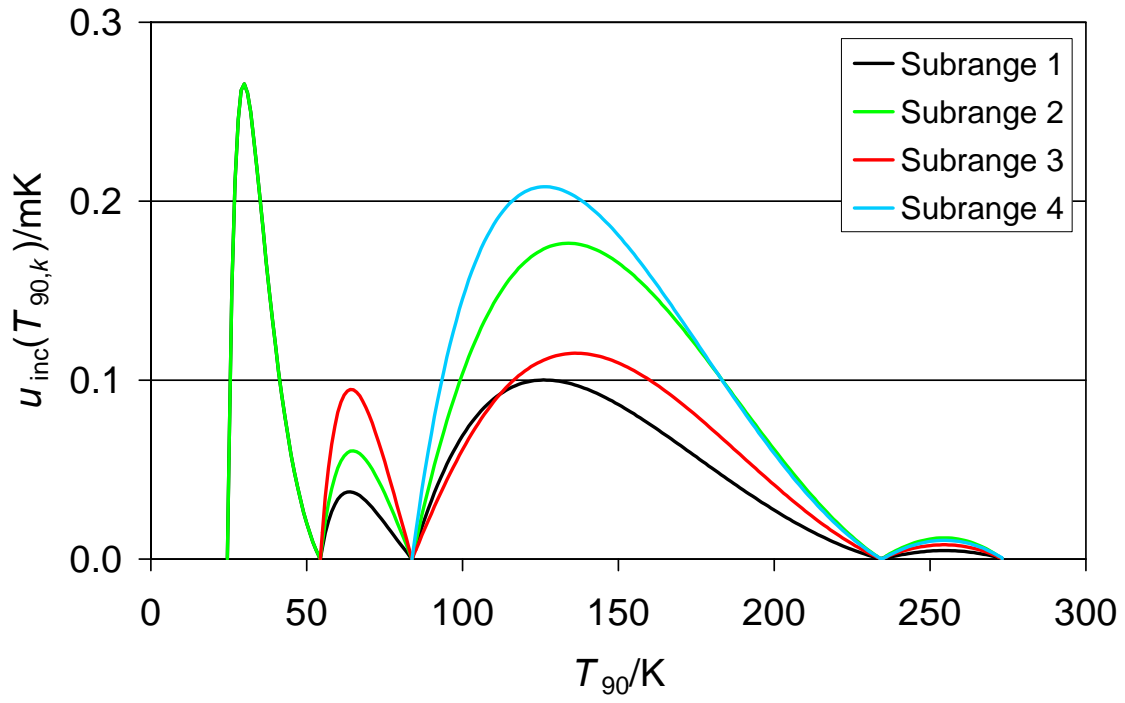


Figure 10

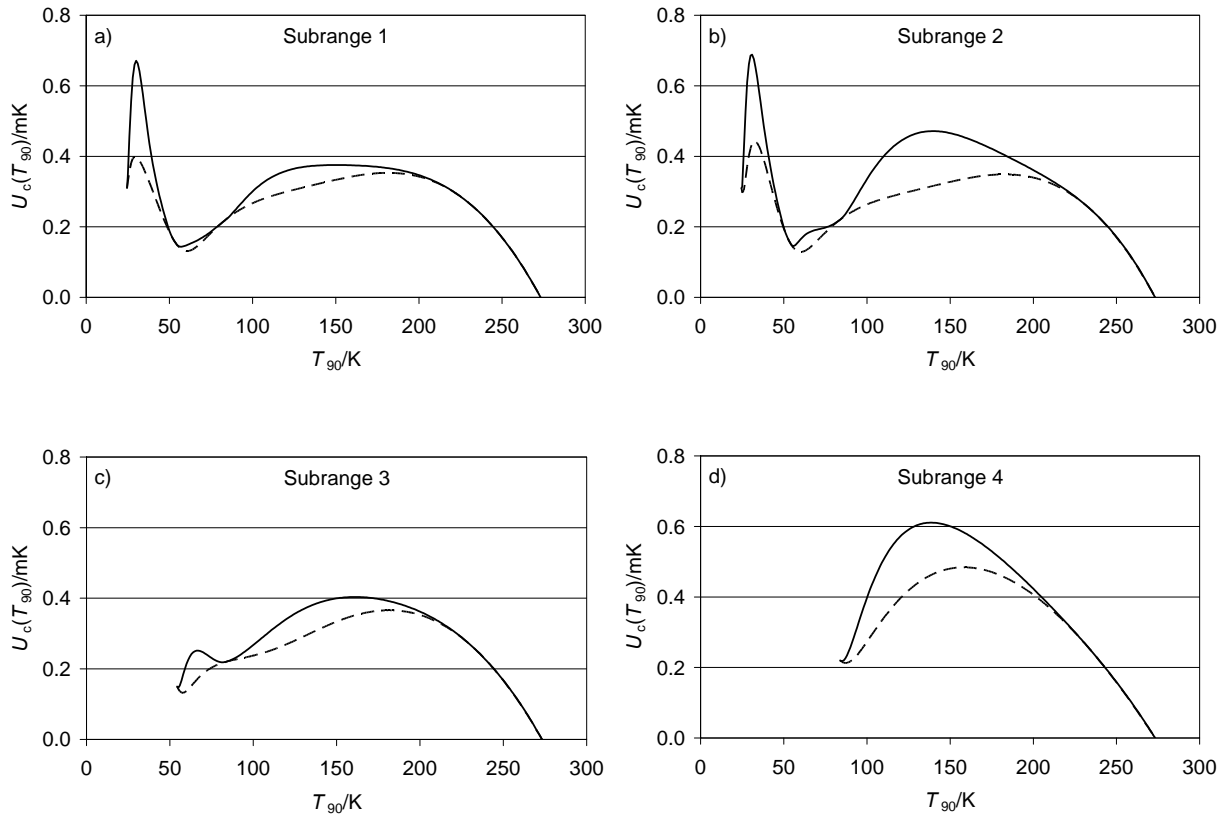


Figure 11